# Environmental noise measurements in Lalitpur area (Kathmandu) after the *M*7.8 Gorkha 2015 earthquake

D. Sandron[1], S. Maskey[2], M. Giorgi[1], D.K. Maharjan[2], S.N. Shrestha[2], C. Cravos[1] and F. Pettenati[1]

[1] *Istituto Nazionale di Oceanografia e di Geofisica Sperimentale - OGS, Trieste, Italy*
[2] *National Society of Earthquake Technology, Kathmandu, Nepal*

ABSTRACT    In the framework of a scientific collaboration with the National Society for Earthquake Technology, Nepal, after the *M*7.8 Gorkha earthquake on 25 April 2015, the National Institute of Oceanography and Experimental Geophysics, Italy, organised a geophysical survey at Kathmandu, in order to have a better understanding of the seismic response of the valley in which the city is located. The main goal was to improve the knowledge of the spectral amplification of the ground motion, due to the fluvio-lacustrine sediments that constitute the Kathmandu basin, by combining the noise ratio H/V technique and velocity dispersion curve analysis. Ambient noise recordings were performed mostly in the Lalitpur area as a single station, and also by an array using ReMi measurement. This study mainly investigates the southern part of the city that was not covered by previous studies. In order to assess the resonant conditions of the soil foundation, microtremor measurements were also performed at Swayambhunath (Monkey Temple) hill and a site close to Boudhanath Stupa, the two prominent Buddhist temples-cum-monasteries that had suffered significant damage during the Gorkha earthquake. The results show that the frequencies at the bottom of the basin are apparently lower than previous surveys and consequently also its depth would be greater.

## 1. Introduction

### 1.1. An earthquake prone area

Lesser Himalaya is the region between the Main Boundary Thrust (MBT) and the Main Central Thrust (MCT), the oldest surficial expressions of the Main Himalayan Thrust (MHT) which is the contact of the underthrusting of India beneath the Asian continent (red lines in Fig. 1). The shallow-dipping MHT detachment allowed the growth of the Himalaya with a series of listric crustal ramps from the base of the detachment to the surface (Fig. 1). The southernmost thrust (the youngest) is the ramp of the Main Frontal Thrust (MFT), the most active from the beginning of the Pleistocene up to now (Amatya and Jnawali, 1994). Models of the seismic coupling show that MHT is locked with the active surface portion MFT (Ader *et al*., 2012; Bollinger *et al*., 2014), but recent simulations suggest that the southern part of the MHT is fully locked during interseismic periods (Jouanne, 2015).
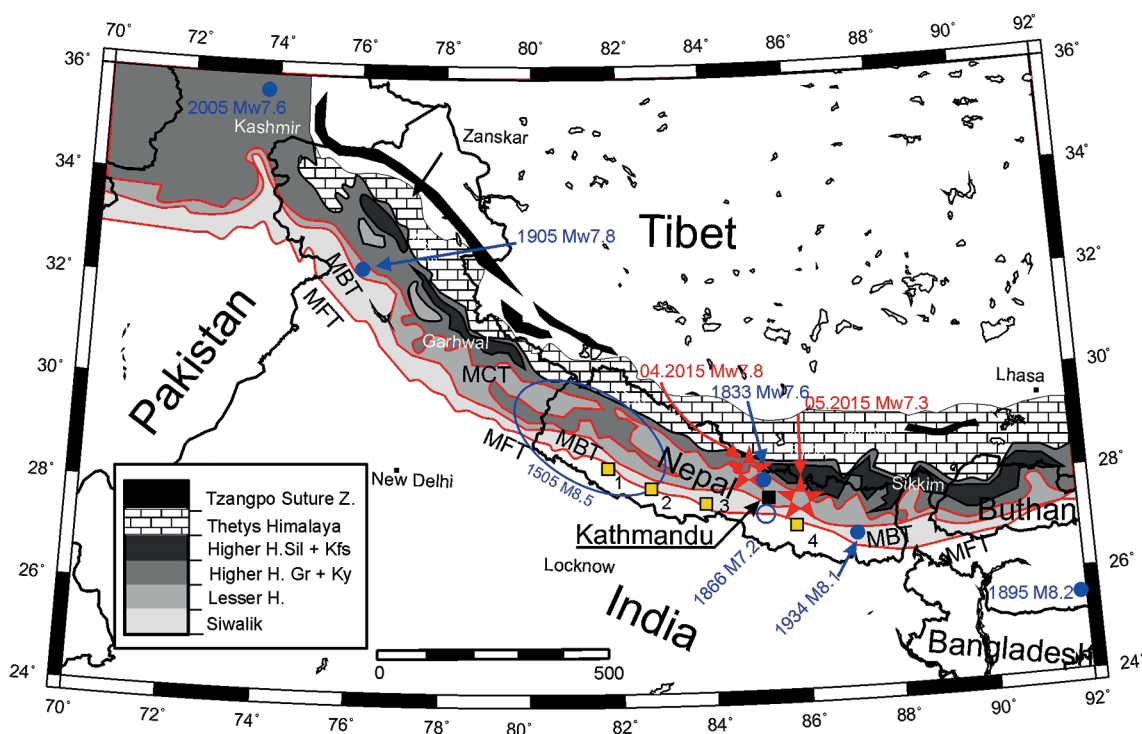
Fig. 1 - Tectonic and geological simplified map of Himalaya. Red curves define the MHT. Red stars: 25 April 2015 $M_w$7.8 Gorkha earthquake and 12 May 2015 $M_w$7.3 aftershock. Solid blue circles: main historical earthquake epicentres. Blue unfilled circle: the doubtful location of 1866 earthquake. Yellow squares indicate the positions of trenches: 1 = Hossler *et al.* (2015); 2 = Mougnier *et al.* (2005); 3 and 4 = Wesnousky *et al.* (2017).

Kathmandu valley is a tectonic intermontane basin developed within the Kathmandu Nappe. It is part of the Lesser Himalayan belt (Stöklin and Bhattarai, 1997) in central Nepal (Fig. 1). Starting from the late Pliocene period, the basin was filled by fluvio-lacustrine sediments until the Quaternary. The basin formations (Sakai *et al.*, 2001, 2008), in ascending order, are: Dharmasthali, Kalimati, Gokarna, Thimi, Tokha, and Patan. Patan (also called Lalitpur) is composed of fluvial deposits which date back from 14-19 kyr (Paudayal, 2011) to 10 kyr (last glaciation) whereas, Gokarna started from the Middle Pleistocene. The age of Kalimati, made up of lacustrine sediments, is 2.8 myr (late Pliocene) – 30 kyr (Pleistocene). Kalimati, termed "black mud" in Nepali, is mainly composed of black organic clay, silts, sand, and gravel, and it is the only formation distributed in the central basin. The formations have a depth of 650 m (Moribayashi and Maruo, 1980) in the central part, overlaid by meta-sedimentary bedrock of Phulchauki Group (Precambrian - Paleozoic) in the southern and central part; gneiss, schists, and granite dominate the north slope.

Kathmandu valley is also a densely urbanised area, with a population of nearly 5 million, exposed to seismic risk deriving from the Himalayan destructive earthquakes (Fig. 1). First record of damage in the Kathmandu valley was due to the huge earthquake of 7 June 1255 (Sapkota *et al.*, 2013; Bollinger *et al.*, 2014, 2016). The valley underwent a severe destruction, with one third of the population killed, including the king, Abhaya Malladeva (8 days later). King Ari Malla also died after the 14 September 1344 earthquake that caused heavy damage in the area,

though no causalities were reported. Other earthquakes causing major damage in the area took place in: 1408, 1681, 1803, 1810, and 1866 (Pandey *et al*., 1995; Szeliga *et al*., 2010). The 1408 event is doubtful and still raises debate among historians due to the lack of sources from that period (Bollinger *et al*., 2016). For the great earthquake of 6 June 1505, notwithstanding the reports by witnesses indicating that it affected an area of about 600 $km^2$ of Himalaya (assessed magnitude about 8.5), NW of Kathmandu, there are no mentions of damage in the Kathmandu valley (Bollinger *et al*., 2016). According to Bollinger *et al*. (2014), the 4 June 1808 earthquake destroyed buildings in Bhaktapur but other authors have not mentioned this event. Another significant earthquake for the Kathmandu valley occurred on 26 August 1833 (Pandey *et al*., 1995), with a magnitude of 7.7 according to Bilham (1995), $M_W$ 7.6 according to Ambraseys and Douglas (2004) and, recently, lowered to 7.3±0.1 by Szeliga *et al*. (2010). However, it led to the destruction of numerous temples, devastated more than 4600 houses and caused 500 fatalities. The macroseismic intensity in Mercalli Modified Intensity (MMI) scale was reported as IX in Kathmandu and X in Patan and Bhaktapur (Bilham, 1995). The epicentre was closer to the valley, only 80 km away, compared to the other aforementioned events. Despite being poorly constrained due to insufficient observations, the 23 May 1866 earthquake (*M* 7.2±0.2), also with an epicentre 80 km south of the city (Szeliga *et al*., 2010), was felt in the Ganges plain, Bihar, Gyirong, and in NE Kathmandu (Bollinger *et al*., 2014, 2016). The macroseismic intensity, around Kathmandu, attributed to the 12 June 1897 Shillong earthquake, occurred more than 600 km from the city, was equal to V on the Medvedev, Shonhever Karnik (MSK) scale (Ambraseys and Douglas, 2004). The $M_W$ 8.2 Bihar-Nepal earthquake struck on 15 January 1934 (Hough and Bilham, 2008; Sapkota *et al*., 2013; Pettenati *et al*., 2017), just 180-200 km from Kathmandu. It caused damage up to VIII grade on the MSK intensity scale according to Ambraseys and Douglas (2004) and IX on the MMI scale for Bilham (1995).

The recent huge earthquake that hit central Nepal on 25 April 2015 at 06:11 UTC registered $M_L$ 7.6 and $M_W$ 7.8 with its epicentre 80 km NW of Kathmandu (Barback-Gorkha). It was associated with the movement of MHT (Denolle *et al*., 2015) with a rupture length of at least 140 km, especially eastwards of the epicentre (Bhattarai *et al*., 2015; Galetzka *et al*., 2015), a hypocentre depth down to 15 km and a dip angle less than 10° (Galetzka *et al*., 2015). The main shock was followed by a several aftershocks, 120 events of $M_L$ greater than 4.0 in the first 12 hours (Bhattarai *et al*., 2015), 553 in 45 days with a shift towards the east. On 12 May 2015, an aftershock of $M_L$ 6.9 ($M_W$ 7.3) struck the eastern part of the area, about 60 km east of the capital. The total number of fatalities was over 8000, more than 22,000 were injured and 790,000 buildings were damaged (MoHA, 2015). The damage in Kathmandu area was assessed between VI and VII degrees on the European Macroseismic Scale (EMS) intensity scale (Dixit *et al*., 2015, NSET, 2015). Galetzka *et al*. (2015) reported that the damage to the vernacular dwellings in Kathmandu was much less than expected for the nearness of the epicentre and the great magnitude. In spite of the closer epicentre and higher magnitude, taller structures like Dharahara Tower (60 m), that partially survived the 1934 earthquake, collapsed. After the 1934 event, 20% of the buildings in the valley were destroyed, whereas the statistics of destroyed buildings indicated only about 1% after the 2015 Gorkha earthquake (Galetzka *et al*., 2015). For completeness, relevant earthquakes in the Himalaya region are also Kangra $M_W$ 7.8, 1905 and Kashmir $M_W$ 7.6, 2005, outside the Nepali area (Fig. 1).

As mentioned, also after the Gorkha earthquake, the geophysical and geodetic data by Avouac *et al*. (2015), along with the recent findings by Bollinger *et al*. (2016), Wesnousky *et al*. (2017)

and the geological trenches, confirmed the locked portion of MHT (SW of Kathmandu) exposes the city to future earthquakes. The positions of some trenches mapped in 2015, and before, are reported in Fig. 1 as yellow squares regarding studies connected with the 1505 earthquake [squares 2 and 1 (Mougnier *et al.*, 2005; Hossler *et al.*, 2015), respectively] and with the 1255 event [squares 3 and 4 (Wesnousky *et al.*, 2017)]. Now this area is locked. Bollinger *et al.* (2016) point out a similarity between the late sequence of earthquakes occurring in 1833, 1934, and 2015 with the 1255, 1344, and 1408 events. The 1833 and Gorkha earthquakes occurred in the same area as the 1344 and 1408 earthquakes. The 1344 event was very destructive and a larger event was expected than the Gorkha $M_W$7.8. Wesnousky *et al.* (2017) support the idea that trenches 3 and 4 ruptured simultaneously, possibly after the 1255 earthquake. In the light of the seismic gap and ~20 mm/year shortening, they speculate that the Gorkha earthquake was not able to break the area between trenches 3 and 4 (about 200 km). According to them, the locked portion is within the area affected by the *M* 8.5, 1505 and *M* 8.2, 1934 earthquakes.

## 1.2. Seismic monitoring activity

In 2012, a large ambient noise survey in the Kathmandu area was carried out (Paudyal *et al.*, 2012, 2013) in order to detect the fundamental periods of vibration and to map the thickness of the basin. The survey almost completely covered the urbanised area but excluded the southern Lalitpur zone. The Japanese portable velocimeter "NewPIC", recording at each point only 5 minutes of background noise with sampling frequency of 100 Hz, was used. Soon after the Gorkha earthquake, Molnar *et al.* (2017) undertook some surveys in the same area with Tromino®, one of the two instruments used in this work.

During the Gorkha seismic crisis there were some accelerometers operating in the Kathmandu area (Fig. 2). Four stations are installed in the southern part of the city, nearly at the same latitude, on the first floor of reinforced public buildings: KTP (Kirtipur Municipality Office, Kirtipur), TVU (Central Department of Geology, Tribhuvan University, Kirtipur), PTN (Pulchowk Campus, Institute of Engineering, Tribhuvan University, Patan), and THM (University Grants Commission Office, Sanothimi, Bhaktapur) (Takai *et al.*, 2016). KTP is located on rock, while the other three on lake sediments of the valley. In the northern urban area, there are two accelerometers installed in the Department of Mines and Geology (DMG) (Bhattarai *et al.*, 2015) and in Kanti Path (NQ. KATNP) (Dixit *et al.*, 2015), managed by the U.S. Geological Survey. The strongest recorded horizontal peak ground acceleration for the main shock was 0.255 g at KTP station, about 0.16 g for NQ.KATNP, while the strongest acceleration on the vertical component was 0.21 g at DMG station. However, all these accelerations were smaller than those expected by GMPE attenuation relations for the Himalayan region (e.g. Singh *et al.*, 1996; Dixit *et al.*, 2015). *PGV* values, instead, are more consistent with predictions. Dhakal *et al.* (2016), instead, highlight that the GMPE relations underestimate the ground motion for periods around 4 s.

Response spectra of Gorkha 2015 strong ground motion data, show a large and wide peak around T = 4 s (Dixit *et al.*, 2015; Bhattarai *et al.*, 2016; Takai *et al.*, 2016; Rupakhety *et al.*, 2017). Initially, Dixit *et al.* (2015) explained this peak at NQ.KATNP station as a source effect, because the periods of the basin, according to Paudyal *et al.* (2012, 2013), do not exceed T = 2 s. They, then, concluded that it could be an effect of non-linearity. Rupakhety *et al.* (2017) through a wave polarization and H/V study on the 5 (TVU, PTN, THM, NQ.KATNP, and KTP) station data claim that the peak around T = 4 s is also a basin effect. Furthermore, these authors indicate
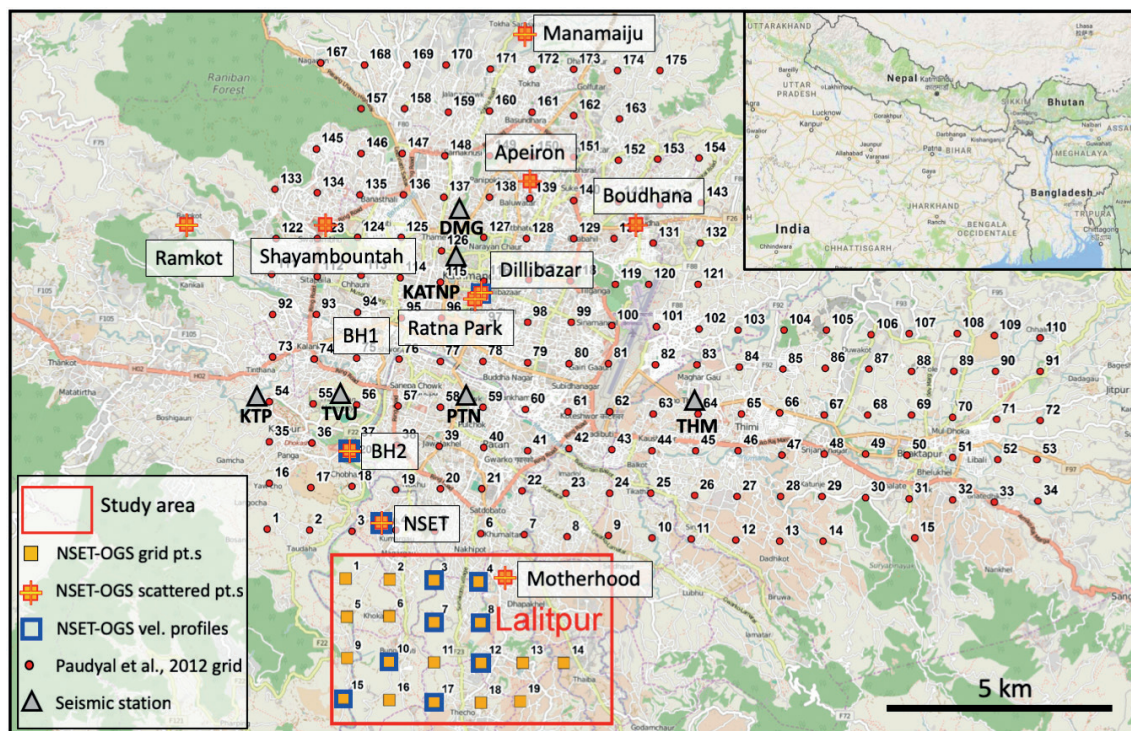
Fig. 2 - Kathmandu urban area map and Nepal geographic position (top right box). Red box: study area. Large orange squares: NSET-OGS planned grid survey points; solid orange squares with crosses: supplementary single measurements points. Blue squares: ReMi surveys. Small numbered solid red circles: Paudyal *et al.* (2012, 2013) survey sites. Grey triangles: seismic stations.

a second peak around T = 0.5 s. The same conclusion was made by Dhakal *et al.* (2016). Fig. 3 shows the response spectra (5% damping) of the horizontal components of the main shock recorded at TVU, PTN, THM, KTP stations. The T = 4.25 s peak is evident at the THM station,
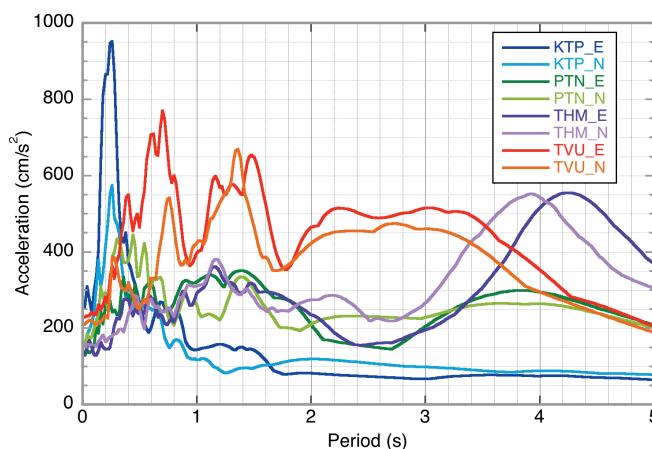


Fig. 3 - Response spectra (5% damping) of the 25 April 2015 $M_w$7.8 Gorkha earthquake horizontal components recorded at KTP, PTN, THM, TVU seismic stations (data from Takai *et al.*, 2016).

but less evident at PTN station. At TVU station, a large peak instead is spread between 2 and 3.5 s. In the KTP recording, long period peaks are missing confirming that it is not a source effect (data from Takai *et al.*, 2016).

In a recent study, Bhattarai *et al.* (2016) analysed the signal spectral ratio (nine 2011-2013 earthquakes) between DMG and the two reference stations of KKA (set at north of Kathmandu on granite/gneiss, 12 km NW of DMG) and PKIN (installed south of Lalitpur, 7 km SE of site 19). On the valley's lake sediments, the study indicated that the amplifications on the 4-10 Hz band are underestimated.


## 2. Methods and instrumentation

### 2.1. HVSR method

The frequency peak, obtained from the ratio between the Fourier amplitude spectra of the horizontal (H) to vertical (V) components of the ambient noise vibrations recorded at a single station (HVSR), is one of the most widely used methods for site-effect studies. This technique was originally proposed by Nogoshi and Igarashi (1971) and disseminated by Nakamura (1989). A review of this method and its application in local effects studies can be found in Otha *et al.* (1978), Lermo *et al.* (1988), Field and Jacob (1993), and a more recent tutorial by Bonnefoy-Claudet *et al.* (2006a). Both the modelling of Fäh *et al.* (2001) and Bonnefoy-Claudet *et al.* (2006b), along with the experimental mixed theoretical studies of Konno and Omachi (1998), demonstrated that Rayleigh and Love waves, and their higher modes, closely control the spectral amplitudes of HVSR. The bodywaves come into play only when there are strong contrasts of impedance, and for frequencies lower than S-wave resonance frequency (Lachet and Bard, 1994). Lunedei and Albarello (2009) concluded that the HVSR are highly sensitive to anelastic properties of the sub-soils. Carcione *et al.* (2016) studied the effects on S-wave amplification function and found that it does not have any significant effect on the peak location. On the other hand, the impedance contrast between the layer and bedrock strongly affects the resonance frequencies. There is also the phenomenon of non-linearity between weak and strong motions that can shift the peaks towards lower frequencies (Otha *et al.*, 1978; Lermo *et al.*, 1988). Regarding the peak amplitude, and in general to quantify the amplification factor of a site, the debate is still open (Konno and Omachi, 1998).

To record the background vibrations of the soil, the National Society of Earthquake Technology, Nepal (NSET) and the National Institute of Oceanography and Experimental Geophysics, Italy (OGS), in cooperation (NSET-OGS) used two types of instruments. For a single station HVSR survey, the tromograph Tromino® and the velocimeter Trillium® were selected. The choice of these instruments was driven first by logistic difficulties because they are light and portable. The former is equipped with two triplets of orthogonal sensors, velocimeters and accelerometers, manufactured by Moho (Italy) with proper period T=1 s, 128 Hz of sampling rate. 40 minutes was the Tromino® standard recording time window. The latter is a three component seismometer with proper period T=20 s, 100 Hz of sampling rate, manufactured by Nanometrics (Canada). A time window of 1 hour was set for the Trillium®.

Tromino® and "NewPIC" (Paudyal *et al.*, 2012) are very similar thereby allowing useful result comparisons. Conveniently, Trillium® allows, instead, a deeper analysis in a broader range of frequencies than Tromino®. A comparative study in the site response estimation between

H/V curves after the data analysis recorded by different sensors is described by Parolai *et al*. (2001).

The SESAME European Project (2004) standardised the H/V method, currently the most common technique to experimentally assess the subsoil resonance (i.e. amplification) frequencies. Further, it has developed the open-source Geopsy® software (www.geopsy.org, last accessed November 2018) that we utilised to analyse the data. We standardised a processing data procedure for each site as: low-noise of 60 s, 3-component signal time windows selected through a short-term average (STA)/long-term average (LTA) anti-trigger with 1 s STA, 30 s LTA and low and high-threshold of 0.2 and 2.5 (to remove the transients and to keep the most stationary parts of ambient vibrations). A 5% cosine taper is applied to both ends of each time window for each component. The spectrum of each component of individual window is smoothed according to the Konno and Omachi (1998) method using a constant of 40. Then, H/V in each window is computed by merging the horizontal (N-S and E-W) components with a quadratic mean. Finally, H/V is averaged over all selected windows.

### 2.2. Velocity measurements through ReMi analysis

Multichannel techniques can essentially be grouped in two groups: 1) techniques based on the arrival time of seismic waves (P or S), 2) techniques based on the spatial correlation of the active (i.e. produced by a known source) or passive (i.e. produced by ambient sources) signals among the receivers (dealing essentially with surface waves). We applied the second type of techniques for several reasons: a) they provide estimates of the shear wave velocity ($V_S$) with no need to generate S waves on purpose; b) they can provide information at deeper depths (compared to refraction surveys); c) they provide curves that are particularly suited to be inverted or fitted together with the H/V curves. In this study, we apply the passive noise ReMi (Refraction Microtremors) technique (Louie, 2001) to gather wave velocities information from Rayleigh wave phase velocity $V_R$ spectra (dispersion curves). The SoilSpy Rosina® equipment, an ultra-portable multichannel digital seismic acquisition system was used. It is composed of a data transmission wire (50 m) along which the amplification/digitalisation modules are deployed (5 m step) and transmits the data from sensors (10 geophones). A proprietary software Grilla® (Castellaro, 2016), part of SoilSpy Rosina®, is installed on a portable PC and allows the acquisition and the pre-processing of the array data. The geometry of the array was always with the geophones sorted on a line. Due to the length of the available wire, our resolution power remained rather shallow (depth ≤ 25 m).

### 2.3. NSET-OGS survey arrangements

In light of the above mentioned seismic hazard conditions, for an expanding city like Kathmandu, the home for great monumental heritage structures under UNESCO supervision, NSET and OGS in the fifteen-day framework of a scientific collaboration in November 2015, organised a geophysical survey by ambient noise measurements mainly in the area of Lalitpur, which was not covered by previous studies. The Lalitpur area was chosen because apart from being covered by delta fan sediments unlike to the north, it is subject to new urbanisation and was damaged during the Gorkha earthquake (Dixit *et al*., 2015; Bhattarai *et al*., 2016).

Paudyal *et al*. (2012, 2013; here after Paudyal Survey Work, PSW) enclosed the northern and the central part of the Kathmandu valley with 172 microtremor data acquisition on a 1 km$^2$ grid points (small numbered solid red circles in Fig. 2), hereafter PSites. NSET-OGS focalised their

activity starting 1 km below the south-western part of Paudyal's network, completing the grid towards the southern urbanised area. The survey was split into a set of 19 HVSR on a grid of 1 km step (large orange squares in Fig. 2) and some spread measurements in the central-northern part of the city (solid orange squares with yellow crosses in Fig. 2). NSET-OGS performed a total of 29 site measurements by Tromino® and 23 by Trillium®. Lalitpur, being a rural area with complex topography, made it tougher to reach the exact location. After a planning session, and once in the field, the grid underwent minor modifications, without causing significant differences to the plan of Fig. 2.

The other spread single measurements were performed in locations close to some prominent buildings or monuments, namely outside the NSET headquarters, 3 sites along the base to the top of the Monkey Temple hill, Boudhanath, Ratna Park, Dilli Bazar and near two Onlus/orphanages (Apeiron and Motherhood). Due to the availability of the soil stratigraphy as a possible benchmark for interpreting the results, a site was chosen very close to the borehole BH2 described in Paudyal *et al.* (2013). In this site and in other 10 sites (blue empty squares in Fig. 2), SoilSpy Rosina® array survey was also performed with the aim of assessing an S-wave phase velocity model.

## 3. Results

### 3.1. HVSR Tromino® data

Fig. 4 shows all the H/V spectral ratio curves after analysing the data recorded by Tromino® (thick blue line) on BH2, NSET headquarters and the first 10 grid points (Fig. 4a); from 11 to 19 grid points (Fig. 4b) respectively. In the frequency range between 0.1-10 Hz, the curves are the average value of the 60 s signal time window along with the one standard deviation band (shading in grey). In the opinion of the authors, after some laboratory tests, 0.5 Hz is the lower frequency boundary of Tromino®. Between 0.5 to 1 Hz, the sensitivity of the instrument depends on strong impedance conditions. Looking at the Tromino® recordings, most of the sites show a rather flat H/V ratio curve with no clear peaks. Site BH2 shows a clear and reliable peak at about 0.69 Hz. Similarly, towards the south, sites 1, 2, 4, 5, 7 (but with high standard deviation), 16 and 17 have distinguishable peaks at 0.51, 1.20, 0.72, 1.82, 0.88, 1.30, and 0.88 Hz, respectively. Less evident are the peaks of sites NSET, 6, 10, 15 and 19, while site 14 has a spike around 2.10 Hz. This peak could have an anthropic origin. Not far to the south of this site, there is a concrete batching plant (ascertained *in situ*).

On Fig. 5, as regards Swayambountah hill (Monkey Temple), that suffered significant damage to the main monastery, the fall of a small temple, and the collapse of one of two free-standing columns, the HVSR curve on the top and on the middle hill are flat, though a wide peak appears in the range 2.8–5.0 Hz at the base. This value can be compared to that of PSite 123 (Fig. 2), which has a peak frequency of 2.8 Hz. At the Boudhanath temple, that reported damage to the top tower, the HVSR curve shows a slight peak around 0.4 – 0.7 Hz, far from the 1.07 Hz of PSite 142. Other sites with interesting measurements are: Dillibazar (0.35 Hz), close to PSite 116 (0.49 Hz) and Ratna Park (0.26 Hz). ONG Apeiron venue has a blunt but evident peak at 0.76 Hz not far from PSite 139 (0.62 Hz). Manamaiju (0.79 Hz) and Ramkot (1.88 Hz), individual points outside the survey area, reported sand liquefaction after the Gorkha earthquake.

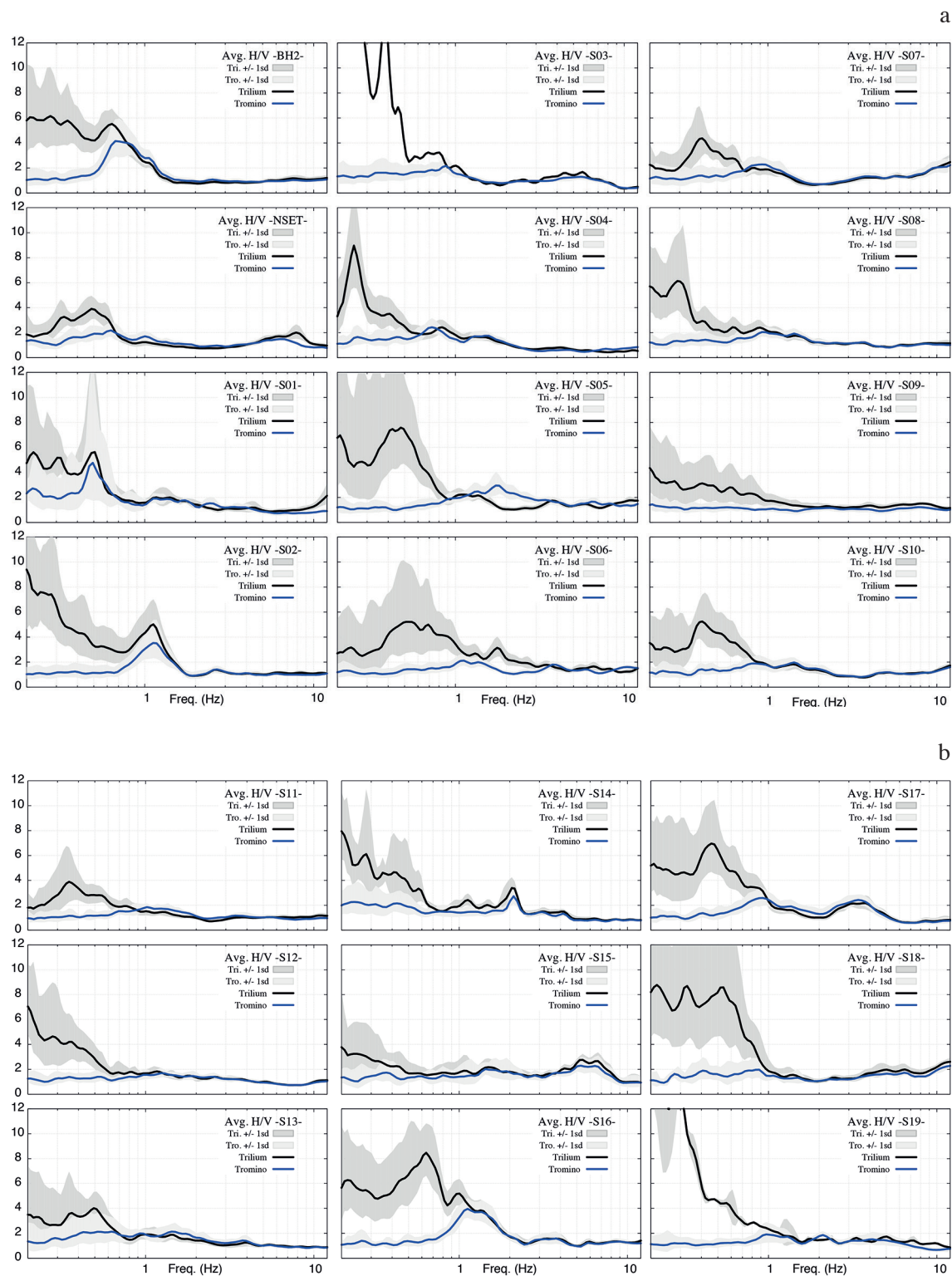All the frequencies of the recognised peaks are listed in Table 1.

Fig. 4 - Average H/V spectral ratio curves resulting from: a) BH2 site, NSET headquarters and 1 to 10 NSET-OGS grid points; b) 11 to 19 NSET-OGS grid points. The grey transparent band defines the one standard deviation range. Thick blue lines: Tromino® data. Thick black lines: Trillium® data.
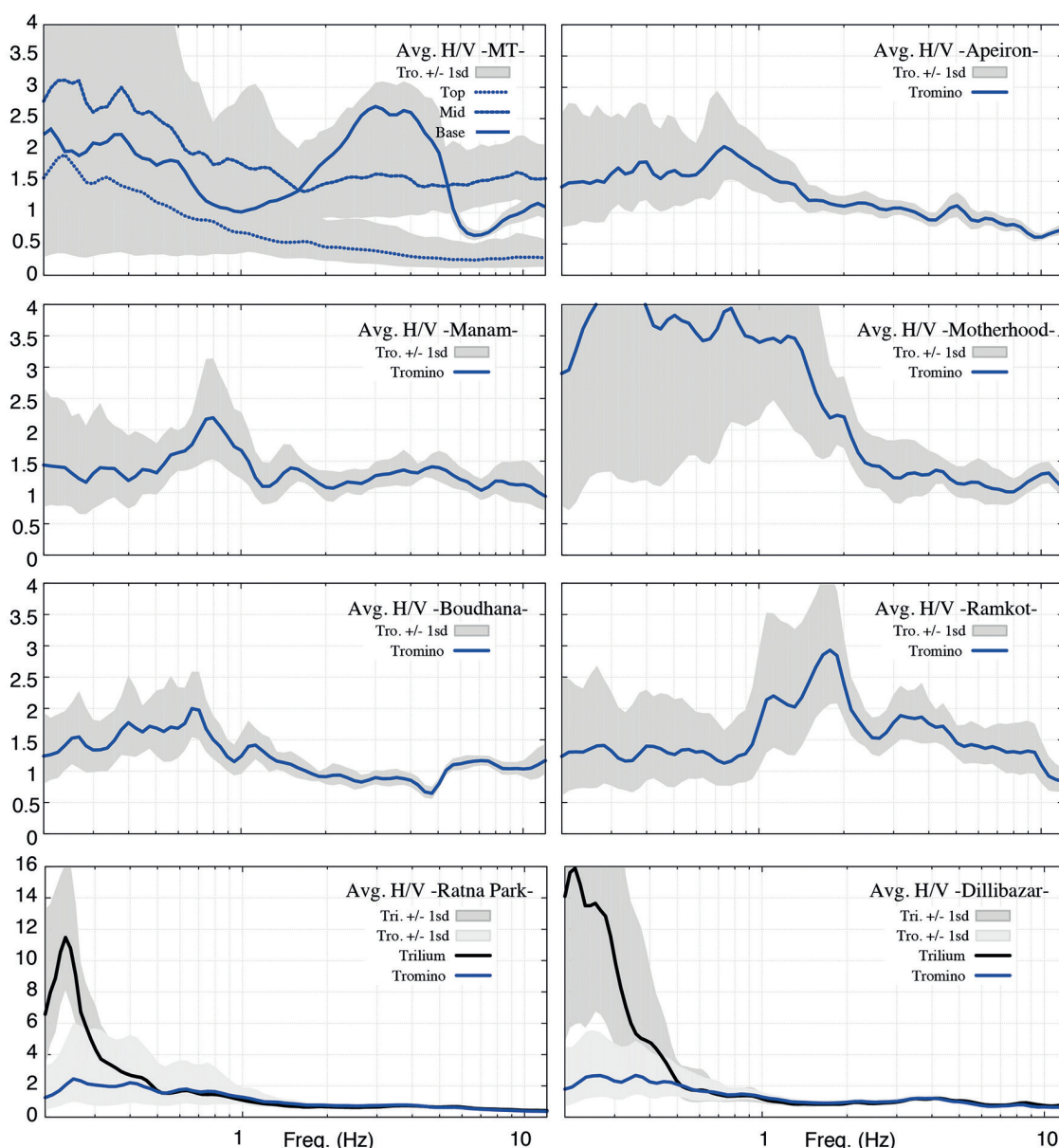
Fig. 5 - Average H/V spectral ratio curves resulting from Monkey Temple (top, middle, base in the same frame); Manam; Boudhanath; Ratna Park; Apeiron; Motherhood; Ramkot, and Dillibazar. The grey transparent band defines the one standard deviation range. Thick blue lines: Tromino® data. Thick black lines: Trillium® data.

Fig. 6a shows on a map the periods of the resulting peaks at the NSET-OGS survey points (Tromino® data) along with those at PSites in PSW. The choice to plot the periods was to avoid the problem of positive skewness of the representation in frequency (Trevisani *et al.*, 2017). The BH2 resonant period (T = 1.45 s) is almost the same as the PSite 37 (T = 1.47 s) in PSW. For the NSET headquarters site, instead, the value (1.61 s) is not fully comparable to that obtained by averaging PSites 4, 5, 19 and 20 (0.72 s).

As expected, on the interpolating map (Fig. 6a), the main resonant periods of the two study areas are undistinguishable, being made at the same time, in the same way, with a similar

Table 1 - HVSR main resonant frequency (frequency ± 1 standard deviation) and peak amplitude (amplitude ± 1 standard deviation) on the NSET-OGS survey points according to Tromino® and Trillium® data after Geopsy® analysis. Paudyal *et al.* (2012, 2103) resonant frequency on the closest sites are reported as well.

| Site | Tromino® | | Trillium® | | Paudyal *et al.*, 2012, 2013 |
|---|---|---|---|---|---|
| | Freq. (Hz) | Amp. | Freq. (Hz) | Amp. | Freq. (Hz) |
| BH2 | 0.69±0.09 | 4.1±1.5 | 0.29±0.05 | 5.6±3.2† | 0.68 (PSite 37) |
| NSET | 0.62±0.11 | 2.2±0.6 | 0.49±0.05 | 3.9±0.9 | 1.38‡ |
| 1 | 0.51±0.07 | 4.5±5.6*† | 0.49±0.09 | 5.6±5.1† | |
| 2 | 1.2±013 | 3.5±1.5 | 0.28±0.09 | 4.8±1.7 | |
| 3 | | | 0.37* | 16.0 | |
| 4 | 0.72±0.08 | 2.4±0.6 | 0.26±0.02 | 8.5±4.4† | |
| 5 | 1.82±0.25 | 3.0±1.0 | 0.48±0.06 | 7.3±3.9† | |
| 6 | 1.2±0.17 | 2.1±0.4 | 0.5±0.09 | 5.2±3.6† | |
| 7 | 0.88±0.12 | 2.3±0.5 | 0.41±0.07 | 4.2±1.7 | |
| 8 | 0.95±0.21 | 2.0±0.4* | 0.31±0.05 | 6.0±3.0 | |
| 9 | | | 0.42±0.06 | 3.2±2.1 | |
| 10 | 1.5±0.17 | 2.0±0.4 | 0.41±0.08 | 4.9±1.8 | |
| 11 | 1.03±0.21 | 1.7±0.3 | 0.35±0.07 | 3.8±2.2 | |
| 12 | | | 0.29±0.05 | 4.5±3.3*† | |
| 13 | | | 0.5±0.09 | 3.8±1.1 | |
| 14 | | | 0.28±0.06 | 5.6±4.0*† | |
| 15 | 5.3±0.98 | 2.3±0.6 | | 3.1±2.0 | |
| 16 | 1.3±0.18 | 3.7±0.8 | 0.63±0.08 | 8.1±2.1 | |
| 17 | 0.88±0.17 | 2.6±0.7 | 0.42±0.09 | 6.9±2.8 | |
| 18 | | | 0.53±0.03 | 7.2±5.6*† | |
| 19 | 1.0±0.17 | 1.9±0.8 | 0.3±0.06 | 12.2±18.9*† | |
| Ratna Park | 0.26±0.04 | 2.1±2.5 | 0.26±0.02 | 11.0±4.0† | 0.68 (PSite 96) |
| Dillibazar | 0.35±0.07 | 2.5±1.7 | 0.22±0.03 | 13.5±15.3† | 0.49 (PSite 116) |
| MT, base | 3.0±0.52 | 2.6±0.4 | | | 2.77 (PSite 123) |
| Boudhana | 0.68±0.08 | 2.0±0.5 | | | 1.07 (PSite 142) |
| Motherhood | | | | | |
| Apeiron | 0.76±0.13 | 2.0±0.6 | | | 0.62 (PSite 139) |
| Manamaiju | 0.79±0.08 | 2.2±0.8 | | | |
| Ramkot | 1.88±0.19 | 2.9±1.0 | | | |

(*) $n_c(f_0)$>200 [number of significant cycles] SESAME criteria for a reliable H/V curve not fulfilled
(†) $\sigma_A(f)$<3 [standard deviation] SESAME criteria for a reliable H/V curve not fulfilled
(‡) Average value between PSite 4, 5, 19, 20 of Paudyal *et al.* (2013)

instrument. The border between the two surveys is well connected, with values around T = 1 s in continuity from one survey to the other. In Table 1, the PSW peak frequency values are reported, too. However, the sensors of both surveys, with fundamental period T = 1 s, are not suitable to detect the actual and also the deeper profundity of the basin. Moreover, in our view, only 5 minutes of data acquisition as performed by PSW are far too short and insufficient.
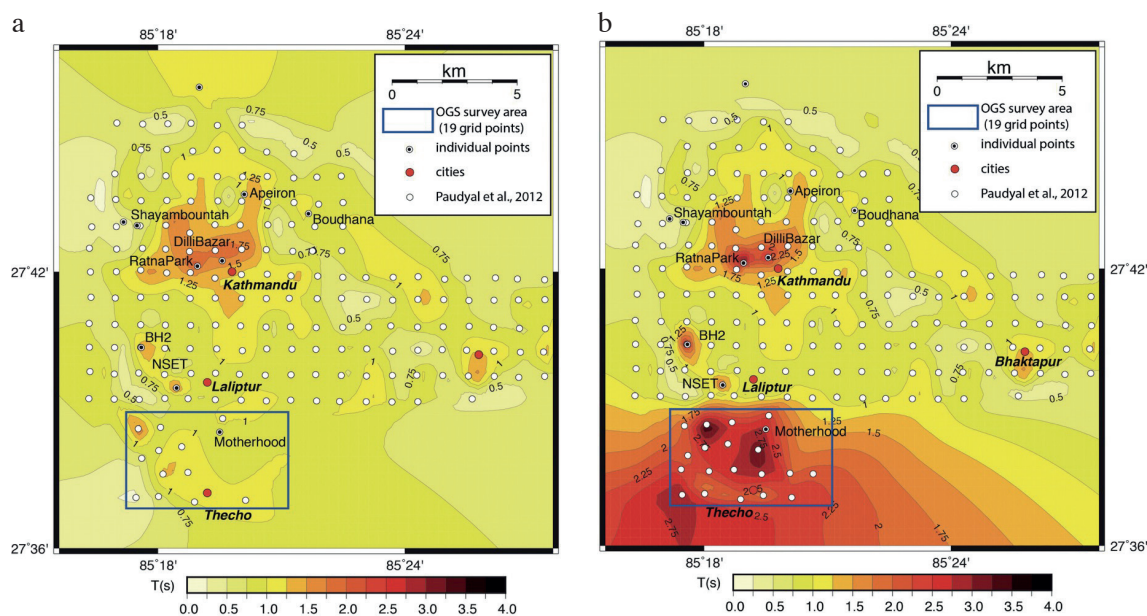
Fig. 6 - Contour map of the HVSR main resonant period by Paudyal *et al*. (2012, 2013) along with those obtained by the NSET-OGS surveys: a) Tromino® data; b) Trillium® data. The Natural Neighbour (Sirovich *et al*., 2002) interpolation scheme is adopted.

### 3.2. HVSR Trillium® 20 data

Fig. 4 shows also all the H/V spectral ratio curves after analysing the data recorded by Trillium® (thick black line), processed in the same manner and with the same parameter setting adopted for the Tromino® recordings. Every Trillium® peak frequency is lower than those obtained by Tromino® data. Most of them are below 1 Hz. On the other hand, the curves of the two instruments match fairly well for frequencies greater than 1 Hz (and sometimes for lower values). Sites 3, 11, 12, and 18, with a flat curve according to Tromino®, have evident frequency peaks below 1 Hz. Site BH2 reproduces the Tromino®'s peak at 0.65 Hz but also shows a peak at 0.29 Hz. This behaviour is also visible at other sites: 1, 2, 4, 7, 10, 16 and 17. At NSET site, the Trillium® curve is equal to the Tromino® one, but below 0.7 Hz there is a shift of the frequency peak. Fig. 5 plots the resulting curves for the Ratna Park and Dillibazar sites. All of the main peaks are below 0.5 Hz. Ratna Park highlights the low frequency peak measured by Tromino® (0.26 Hz), while Dillibazar (0.22 Hz) shows the greatest peak of the survey even if with a very large associated error. These two peak values are in agreement with the long period peaks at the nearby Kanti Path (NQ.KATNP) station (all these sites are in the centre of the basin).

As expected, in Fig. 6b the separation between the areas covered by the NSET-OGS and PSW surveys is clear, the first being marked by longer periods in the southern part with respect to the northern one.

### 3.3. Velocity analysis by SoilSpy Rosina®

As stated above, 11 velocity arrays were done on sites: BH2, NSET, 3, 4, 7, 8, 10, 12, 15, and 17, and in the centre of Kathmandu, close to Dillibazar (Fig. 2). The microtremor H/V curves are indicative of some key features of the subsurface structure: a) the presence of stiff layers
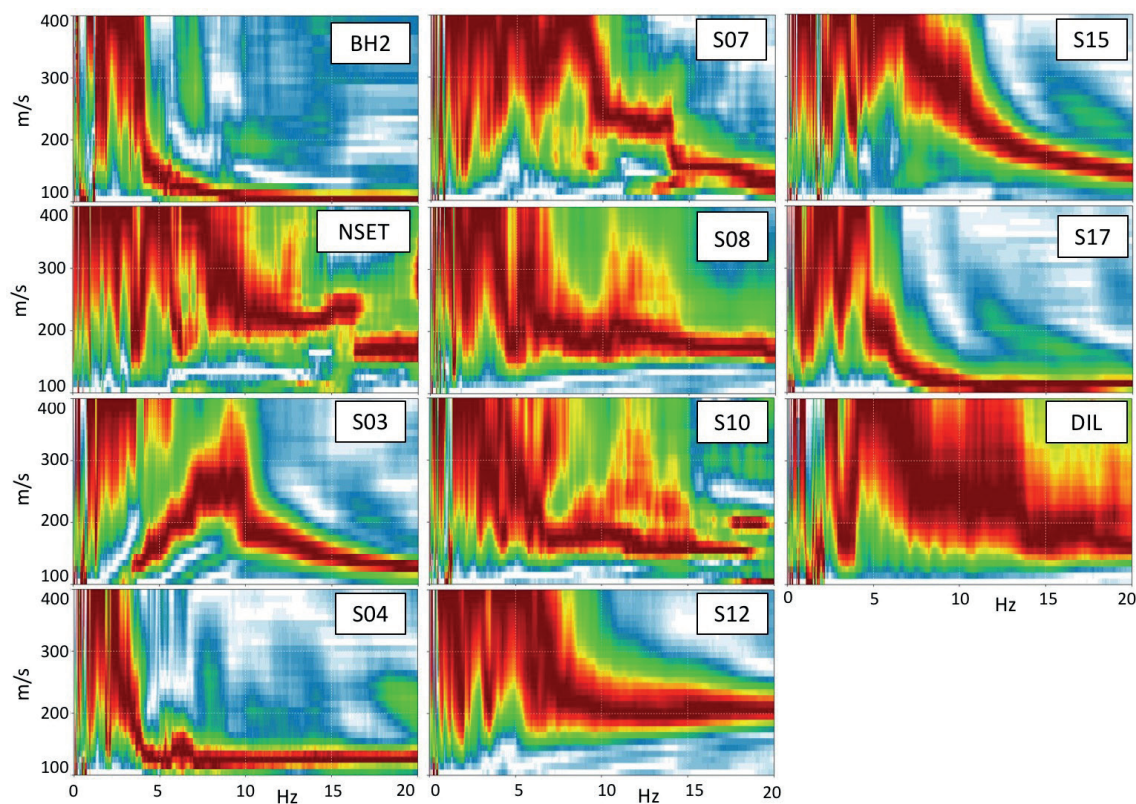
Fig. 7 - $V_R$ spectra for each of 11 NSET-OGS sites where velocity array measurements were performed (Fig. 1).

through the peak amplitudes; b) their relative depth through the peak frequencies (Castellaro and Mulargia, 2009a); c) the presence of lateral heterogeneities if their variation in space are detected and d) velocity reversals (Castellaro and Mulargia, 2009b). Through the analysis of the dispersion properties of Rayleigh and Love waves, it is possible to retrieve $V_S$ profiles. In recent years, the joint fit of H/V and dispersion curves have been proposed by several authors (e.g. Castellaro and Mulargia, 2010, 2014) and $V_S$ profiles matching both the experimental H/V and dispersion curves were considered better constrained than models based on the match of the curve from a single technique. Briefly, the passive (microtremors) multichannel seismic signals were processed in the $V_R$ vs. frequency space to provide the experimental dispersion curves, as shown in Fig. 7, from which one can assess the minimum frequency at which the velocity curve can be defined. Because Rayleigh waves cause the greatest underground displacement at a depth between 1/3 and 1/2 of their wavelength, by dividing the maximum wavelength by 2, it is possible to estimate (for excess) the maximum depth of investigation probably reached by the measure.

Although the $V_S$ are about 10% higher than $V_R$, considering the uncertainties of the measurements especially in the lower velocity range, they appeared to be comparable. A low velocity layer with $V_R$ around 120-160 m/s in the first metres (top soil) is clearly recognizable. BH2 dispersion curve (Fig. 7) at 6-7 Hz shows a hint of velocity reversal, more evident at site 3. This small inversion is visible also at the NSET headquarters, around 15 Hz, marked also on the PS logging stratigraphy of the borehole close to it (Table 2) between 14-16 m. A thin layer with $Vs = 200$ m/s interrupts a

Table 2 -The PS logging stratigraphy and parameters of the site close to NSET headquarters.

| Thick (m) | *Vs* (m/s) | Poisson ratio | Density (103 kg/m³) |
|---|---|---|---|
| 0 ÷ 2 | 100 | 0.450 | 1.5 |
| 2 ÷ 8 | 157 | 0.487 | 1.5 |
| 8 ÷ 10 | 333 | 0.437 | 1.9 |
| 10 ÷14 | 333 | 0.474 | 1.7 |
| 14 ÷ 16 | 200 | 0.490 | 1.9 |
| 16 ÷ 22 | 363 | 0.468 | 2.0 |
| 22 ÷ 24 | 486 | 0.440 | 2.0 |
| 24 ÷ 30 | 313 | 1.700 | 0.5 |

trend of *Vs* over 300 m/s. For sites 8 and 12, the first layer starts with velocity near 180-200 m/s and increases, at 6-7 Hz, to 240-260 m/s (about 16-18 m depth). We can hypothesise that for these two sites the top soil is missing. Also, for BH2 and site 4, at 5-6 Hz, *Vs* are over 220 m/s at 25 m depth. Below the first layer, it is possible to speculate an increase of velocity from 220 to 300 m/s. At sites 15 and 17, a second mode of vibration is visible at about 30 Hz. The Rosina® survey in Dillibazar (in the centre of the urban area), confirms the results obtained for the Lalitpur area.

## 4. Interpretation and discussion

### 4.1. Preliminary data interpretation

Aware of the limited resolution power of the data collected with the array, we do not claim to assess the depth of the basin, but to explain the relation between it and the low frequency H/V peaks resulting from our survey and the long period peaks highlighted by the recorded strong motion data, if any. The tested KTP station (Fig. 2) is installed on rock, with *Vs* over 700 m/s at 10 m depth (Takai *et al.*, 2016). The other three stations (TVU, PTN, THM) are on the lake sediments of the basin with velocities around 200 m/s. These velocity values were taken as our reference. Examining the 11 dispersion curves (Fig. 7), there is clear evidence of a top soil layer with $V_R$ equal to 120–160 m/s. A velocity value in the range 200 – 280 m/s is hypothesised for the layer below. The PS logging stratigraphy of the site close to the NSET headquarters (Table 2) matches the assessment of $V_R$ by SoilSpy Rosina®, i.e. 8 m of top soil and the alternation of layers below with *Vs* 200 and 360 m/s.

The stratigraphy of BH2 (Fig. 8) is very heterogeneous, but according to Paudyal *et al.* (2013) at a depth of 232 m there is the limit between clays and a thick layer of sands. Following to the empirical equation (Paudyal *et al.* 2013)

$$H = 146.01 \, f^{-1.208} \tag{1}$$

for a frequency equal to 0.68 Hz (PSite 37) the rock basement results at 233 m deep (contradicting what is reported about the stratigraphic sequence and what indicated in their picture). The NSET-OGS measurements by both Tromino® and Trillium® (Fig. 4a) highlight a frequency peak at 0.69 Hz. At the borehole BH1 (Fig. 8), located between PSite 75 and PSite 94 of PSW, the basement depth H is equal to 252 m, adopting the frequency of PSite 94 (0.62 Hz) in Eq. 1. But assuming
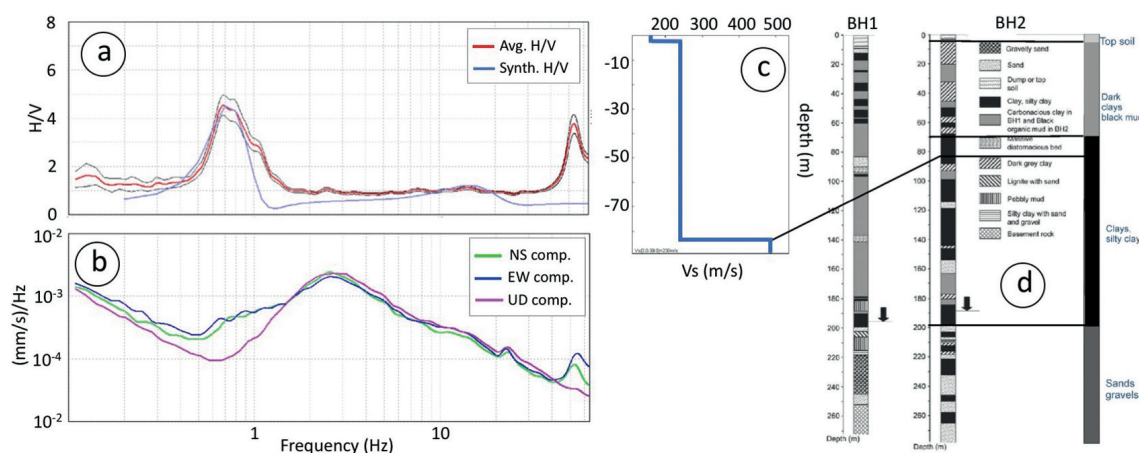
Fig. 8 - Site BH2, Tromino® data. a) Average H/V spectral ratio curve (red line) with one standard deviation (dashed line). The blue line defines the theoretical H/V curve for the subsoil in panel c. b) Recorded spectrum of the 3 components (green = N-S, blue = E-W, violet = vertical) that refers to the spectral ratio in panel a. c) Subsoil sketch modelled by the joint fit of the H/V curve and phase $V_R$ spectra acquired (Fig. 7). d) Stratigraphy of the BH1 and BH2 boreholes modified from Paudyal *et al.* (2013).

that 0.62 Hz is the bedrock frequency, fixing its depth at 252 m, the resulting $V_S$ (=4H$f$) would be equal to 625 m/s, which is compatible with a wet sand/gravels layer. Table 3, for comparison purposes, schematically reports: i) the simplified BH2 borehole stratigraphy; ii) Dhakal *et al.* (2016) model; iii) the model obtained after analysing the Tromino® data; iv) the Hypothesis model (a simplified general interpretation from all available data). The modelling via Grilla® software for BH2 borehole returns two layers: top soil for the first 2.5 m and Dark grey clays with black mud up to 82 m (Fig. 8). According to the borehole BH2 stratigraphy, a huge layer of clay and silty clays starts below 70 m and at 88 m there is the last layer of Dark grey clays of relevant thickness. A change in impedance contrast at the depth around 75–90 m probably occurs. Using the peak frequency model in Table 3 of sites BH2, 1, 2, 4, 5, 7, 16, and 17 (Fig. 4a), a discontinuity map in Kalimati formation depth is proposed (Fig. 9), on the NSET-OGS study area.

Table 3 – Kathmandu basin simplified scheme: i) the simplified BH2 borehole stratigraphy (panel d in Fig. 8); ii) Dhakal *et al.* (2016) model; iii) the model obtained after analysing the Tromino® data; iv) the Hypothesis model.

| BH2 (Fig. 8) | H (m) | Dhakal *et al.*, 2016 H (m) | $V_S$ (m/s) | Tromino® H (m) | $V_R$ (m/s) | Poisson ratio | Density (103kg /m³) | Hypothesis VR (m/s) | Poisson ratio | Density (103kg/ m³) |
|---|---|---|---|---|---|---|---|---|---|---|
| Top soil | 2÷15 | | 200 | 0 ÷ 2.5 | 150 | 0.45 | 1.6 | 100 ÷ 160 | 0.45 ÷ 0.48 | 1.5 ÷ 1.9 |
| Dark grey clays | 30÷60 | 30 | 200 | 2.5 ÷ 82 | 220 | 0.48 | 1.9 | 220 ÷280 | 0.44 ÷ 0.48 | 1.7 ÷ 2.0 |
| Clays – silty clays | 180÷220 | 230 | 350 | $0 | 445 | 0.44 | 2.2 | 300 ÷ 500 | 0.43 ÷ 0.45 | 2.0 ÷ 2.4 |
| Gravels - Sands | | 470 | 500 | | | | | 600 ÷ 630 | 0.40 ÷ 0.42 | 2.1 ÷ 2.4 |
| Basement | | > 470 | 3400 | | | | | > 700 | 0.35 ÷ 0.38 | 2.4 ÷ 2.6 |
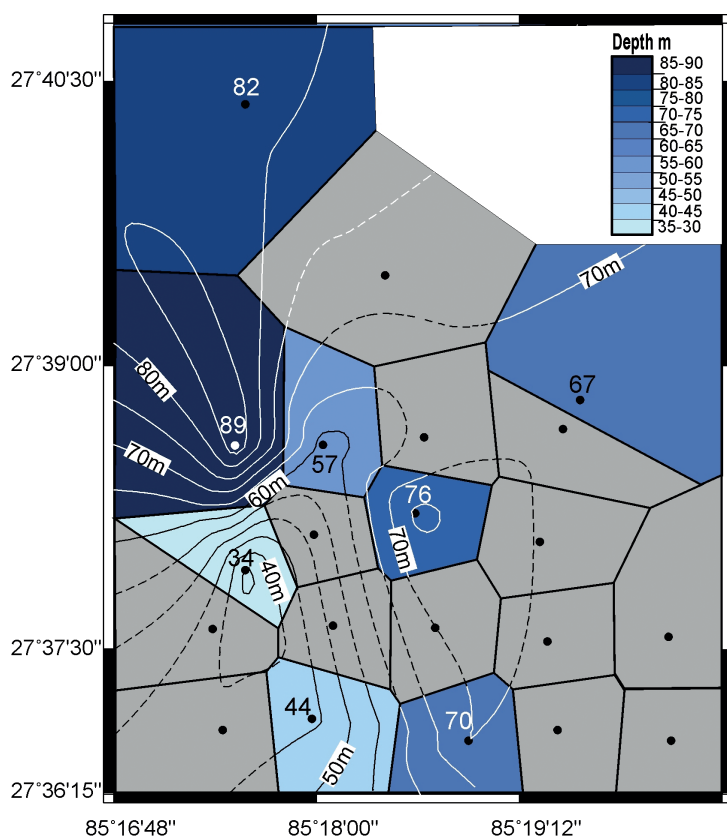
Fig. 9 - Tromino® resonant period tassellation. The Voronoi polygons represent the areas of influence of all sites in the Lalitpur area. Polygons belonging to sites with a clear peak are coloured. Polygons belonging to sites without or doubtful peak are in grey. The associated depth values come from Grilla® modelling. The depth contour lines are defined with the Natural Neighbour (Sirovich *et al.*, 2002) interpolation scheme.

### 4.2. The hypothesis of a discontinuity at 80-90 m depth

Modelling the most prominent peaks of the Tromino® H/V curves and exploiting the velocity information (paragraphs 3.2., 4.1. and Tables 2 and 3), a discontinuity between 50–90 m was encountered (Fig. 9). This surface, variation in depth apart, is surprisingly shallow with respect to PSW interpretations, but considering the range of velocities (and consequent thickness), the trend of top soil layer is rather unique. Fig. 9 shows a hypothesis of the trend of this surface with depth. Voronoi polygons related to all the 19 sites of NSET-OGS survey are coloured by shades of blue as a function of the depth (the depth contour curves are superimposed). The grey polygons enclose the areas with a flat HVSR curve, where the $V_S$ probably increases with slight gradient (Castellaro, 2016), and consequently a discontinuity is not clearly detectable. This gradual increment of $V_S$ is clear in the $V_R$ wave spectra (Fig. 7, curves 3, 8, 12). Site 3 shows a $V_R$ velocity inversion in the first layers. The NSET headquarters HVSR curve (Fig. 4a), with broad and weak peaks on frequencies lower than 0.6 Hz and a not very clear peak at 1 Hz, has a gradual increasing of velocities in the shallower depth, compatible with those reported in Table 2. On the other hand, the same curve obtained with Trillium® data (Fig. 4a) shows a better agreement with the model: the main peak is at 0.49 Hz, a weak prominence at 1 Hz and another high peak at 6-8 Hz (the top soil marker). Probably the 1 Hz prominence is the sign of the layers below the top soil, with a gradual increasing of velocity up to 300 m/s (Table 2). This result also matches well with the findings of Molnar *et al.* (2017).

This sort of discontinuity inside the basin formation, especially in the Kalimati formation, could be due to an increase of the impedance contrast caused by the compaction of sediments after a change in the geological and/or climatological conditions. There are several studies regarding the climate oscillations from vegetation and pollen deposits in the last glacial period concerning the last 50 m of sediment deposits (Fujii *et al*., 2004; Kuwahara *et al*., 2004; Paudayal, 2011). Seven climate oscillations had occurred during the period of older deposits according to Igarashi *et al*. (1988). These oscillations mean that there was an alternation of draining or filling the Paleo Kathmandu Lake with water. In the younger stage (late Pleistocene), the Patan formation was affected by a cold and drier climate (glacial). The confirmation of lake shrinkage in the late Pleistocene age in the southern formations of the basin comes from the $^{14}$C method (Mukunda and Sakai, 2008). In general, the geological studies of the sediments of the basin also show a notable lateral and vertical heterogeneity of the layers with heteropic indentations (Igarashi *et al*., 1988; Dill *et al*., 2001). Mampuku *et al*. (2008) clarified past climate changes through the analysis of $\delta^{13}$ variation of bulk organic carbon, which determines the changes in the $C_{13}/C_{14}$ ratio on vegetation for the last 600 kyr in the Rabibhawan borehole (BH1). Sakai *et al*. (2001) has reported seven cyclical oscillations from middle to late Pleistocene, corresponding to the glacial and interglacial fluctuations. In particular, also using other indicators, the authors focus their analysis on a level of sand from 83 to 89 m deposited at the end of the glacial phase. The principal and most interesting information comes from the core drilled method used: down to 83 m, drilling was carried out by percussion, and by wire-line, especially below 89 m. In agreement with Sakai *et al*. (2001), the deposit of this sand layer was caused by a rapid drawdown of the lake in a short interval of time during a dry/cold period at the end of the glacial phase. In addition, as the result of compaction rates and/or clays dehydration with increasing burial depth, the sedimentation rates of the portion of the Kalimati clay formation appear to increase gradually from the lower to upper part of the sediments except the 83-89 m sand layer.

In our opinion, lacking any specific study for this discontinuity in literature, this type of information can support the intriguing contrast of impedance inside the Kalimati formation.

*4.3. Considerations on basement depth*

It was easily found, that Trillium® was more reliable to reach the rock basement. On the map in Fig. 6a, Tromino® shows two relative maxima depths below site 1 and site 10. According to Trillium® (Fig. 6b), the two maxima are shifted on site 2, site 10 disappears, but there is a maximum on site 8.

Regarding the site BH1, fixed H = 252m and f = 0.62 Hz as reported in the available stratigraphy, a *Vs* = 625 m/s is computed via the well-known equation $V_S$ = 4H*f*. This value could be reasonable in the presence of wet sands and gravels, or of a strong impedance contrast (Bonnefoy-Claudet *et al*., 2006b; Lunedei and Albarello, 2009). Paudyal *et al*. (2013), in their analysis, used the frequency of the PSite 94 (*f* = 0.62 Hz), but in our opinion (Fig. 1), BH1 seems closer to PSite 75 (*f* = 1.05 Hz) than PSite 94. If H = 252 m, the velocity would be 1060 m/s. Applying Eq. 1, given the frequency of PSite 75, the basement depth H would be 138 m. Molnar *et al*. (2017) reports, for two measurements close to PSite 75, two peaks at frequencies 0.62 Hz and 1.05 Hz.

As concerns BH2, having fixed the *Vs* of KTP station (Takai *et al*., 2016) as the velocity of the sediment at the bottom of the lake (625 m/s) and the Trillium® peak of 0.29 Hz, the resulting

depth of the basement would be equal to 539 m. Moreover, introducing the value of the second frequencys peak (0.68-0.69 Hz) in the equation below:

$$H_1 = (V_{S1}/V_{S2}) \times (f_2/f_1)\, H_2 \qquad\qquad (2)$$

where $V_{S1} = 220$ m/s (the velocity of the second layer in Table 2), $V_{S2} = 625$ m/s, $H_2 = 539$ m, the resulting depth $H_1 = 80\text{-}81$ m, which is in perfect agreement with what is reported in Table 3 (82 m). Taking into account the parameter uncertainties in Table 3, the depth $H_1$ ranges from 72 to 105 m. The computed depth H close to BH2 borehole by Eq. 1 and the available frequencies of PSW can vary in a range between 225 to 233 m, but on the available stratigraphy at these depths there is a presence of clays and sands, not bedrock.

Paudyal *et al.* (2012) note that in the central part of the basin, a drill-well encountered the basement rock at 550 m (Khadka, 1993). The location of the drill well is at Bhrikutimandap Exhibition Hall close to the PSite 96 and Ratna Park. The peak frequency of the PSite 96 is 0.68 Hz, the same as for BH2 with a consequent assessment of the depth at 233 m. On the other hand, in the middle of Ratna Park, 200 m away in free field, NSET-OGS measurement reported a Trillium® frequency peak at 0.26 Hz. Given $V_S = 625$ m/s, H = 550 m, the HVSR frequency would be equal to 0.28 Hz. This further confirms the deepest velocity of sediments. Morybayashi and Maruo (1980) reported a maximum depth of 650 m in the centre of Kathmandu basin that corresponds to a frequency of 0.24 Hz. Molnar *et al.* (2017) show some evident peaks for frequencies around 0.3 Hz in Durbar Square. This main square suffered damage to many important temples under UNESCO heritage including the Dharahara Tower. These sites are in the centre of the city and along with Ratna Park, lie in the area where the maximum depths of the basin are supposed to be.

In our opinion, the frequencies measured by Trillium® are more reliable to hypothesise the depth of the bedrock. For higher frequencies, the results of velocity array detections of this study are comparable with MASW survey by Molnar *et al.* (2017) that shows slightly lower $V_R$, less than 200-250 m/s in the shallower sediments.

## 5. Conclusions

The preliminary results of the geophysical survey performed at Kathmandu, aiming to better understand the seismic response of the valley, are presented. The study combined a set of HVSR ambient noise surveys with a set of ReMi array measurements. The study area was mainly focused in Lalitpur in order to complete the analysis performed by previous studies (Paudyal *et al.*, 2012, 2013). For single station HVSR surveys, we employed two types of instruments: the 1 s tromograph Tromino® and the 20 s velocimeter Trillium®.

Tromino®, which is very similar to the instrument adopted by Paudyal *et al.* (2012, 2013), is not suitable to study the full response of the basin. Most HVSR curves for frequencies lower than 1 Hz, flat according to Tromino® data, have evident frequency peaks according to Trillium®. On the contrary, the two lines match fairly well for frequencies greater than 1 Hz.

Notwithstanding the limitations, the passive noise ReMi survey via the SoilSpy Rosina® equipment, allowed us to gather useful $V_S$ information. The joint fit of HVSR and dispersion curves enabled modelling $V_S$ profiles showing a top soil layer (2–15 m) with $V_S$ equal to 160–180

m/s, over a second layer characterised by $V_S$ greater than 220 m/s. These findings are confirmed by borehole stratigraphy.

On modelling the most prominent peaks of the H/V curves around 0.7 Hz, a discontinuity between 80–90 m was encountered in the basin formation that could be due to an increase of the impedance contrast caused by the compaction of sediments after a change in the geological and/or climatological conditions.

The resonant periods detected by Trillium® are between 0.25 to 0.5 Hz. In the middle of Ratna Park, very close to the city centre, NSET-OGS measurement reported a frequency peak at 0.26 Hz compatible with a depth of the basin equal to 550 m.

These values are also compatible with the large and wide peak (around T = 4 s) highlighted on the response spectra of the horizontal components of the 2015 Gorkha earthquake, recorded in some accelerometric stations installed in the city centre.

We do not claim to have assessed the true depth of Kathmandu valley, but our results indicate that the basin frequency/ies is/are supposedly lower than the values described by previous surveys and consequently its depth is greater.

REFERENCES

Ader T., Avouac J.P., Liu-Zeng J., Lyon-Caen H., Bollinger L., Galetzka J., Genrich J., Thomas M., Chanard K., Sapkota S.N., Rajaure S., Shrestha P., Ding L. and Flouzat M.; 2012: *Convergence rate across the Nepal Himalaya and interseismic coupling on the Main Himalayan Thrust: Implications for seismic hazard*. J. Geophys. Res., **117,** B04403, doi: 10.1029/2011JB009071.

Amatya K.M. and Jnawali B.M.; 1994: *Geological Map of Nepal*. Department of Mine and Geology, Lainchaur, Kathmandu, Nepal.

Ambraseys N.N. and Douglas J.; 2004: *Magnitude calibration of north Indian earthquakes*. Geophys. J. Int., **159**, 165-206, doi: 10.1111/j.1365-246X.2004.02323.x.

Avouac J.-P., Meng L., Wei S., Wangand T. and Ampuero J.-P.; 2015: *Lower edge of locked Main Himalayan Thrust unzipped by the 2015 Gorkha earthquake*. Nat. Geosci., **8**, 708-711.

Bhattarai M., Adhikari L.B., Gautam U.P., Laurendeau A., Labonne C., Hoste-Colomer R., Sèbe O. and Hernandez B.; 2015: *Overview of the large 25 April 2015 Gorkha, Nepal, earthquake from accelerometric perspectives*. Seismol. Res. Lett., **86**, 1540-1547, doi: 10.1785/0220150140.

Bhattarai M., Adhikari L.B., Gautam U.P., Bollinger L., Hernandez B., Yokoi T. and Hayashida T.; 2016: *Establishing a reference rock site for the site effect study in and around the Kathmandu valley, Nepal*. Earth, Planets Space, **68**, 81, doi: 10.1186/s40623-016-0454-9.

Bilham R.; 1995: *Location and magnitude of the 1833 Nepal earthquake and its relation rupture zones of contiguous great Himalaya earthquakes*. Curr. Sci., **69**, 101-128.

Bollinger L., Sapkota S.N., Tapponnier P., Klinger Y., Rizza M., Van der Woerd J., Tiwari D.R., Pandey R., Bitri A. and Bes de Berc S.; 2014: *Estimating the return times of great Himalayan earthquakes in eastern Nepal: evidente from the Patu and Bardibas strands of the Main Frontal Thrust*. J. Geophys. Res. Solid Earth, **119**, 7123-7163, doi: 10.1002/2014JB010970.

Bollinger L., Tapponnier P., Sapkota S.N. and Klinger Y.; 2016: *Split deficit in central Nepal: omen for a repeat of the 1344 AD earthquake?* Earth, Planets Space, **68**, 12, doi: 10.1186/s40623-016-0389-1.

Bonnefoy-Claudet S., Cotton F. and Bard P.-Y.; 2006a: *The nature of seismic noise wavefield and its implications for site effects studies*. *A literature review*. Earth-Sci. Rev., **79**, 205-227, doi: 10.1016/j.earscirev. 2006.07.004.

Bonnefoy-Claudet S., Cornou C., Bard P.Y., Cotton F., Moczo P., Kristek J. and Fah D.; 2006b: *H/V ratio: a tool for site effects evaluation. Results form 1-D noise simulation*, Geophys. J. Int., **167,** 827-837.

Carcione J., Picotti S., Francese R., Giorgi M. and Pettenati F.; 2016: *Effect of soil and bedrock anelasticity on the S-wave amplification function*. Geophys. J. Int., **208,** 424-431, doi: 10.1093/gji/ggw402.

Castellaro S.; 2016: *The complementare of H/V and dispersion curves*. Geophys., **80**, 1-16, doi: 10.1190/GEO2015-0399.1.

Castellaro S. and Mulargia F.; 2009a: *Vs30 estimates using constrained H/V measurements*. Bull. Seismol. Soc. Am., **99**, 761-773.

Castellaro S. and Mulargia F.; 2009b: *The effect of velocity inversions on H/V*. Pure Appl. Geophys., **166**, 567-592.

Castellaro S. and Mulargia F.; 2010: *How far from a building does the ground-motion free-field start? The cases of three famous towers and a modern building*. Bull. Seism. Soc. Am., **100**, 2080-2094, doi: 10.1785/0120090188.

Castellaro S. and Mulargia F.; 2014: *Simplified seismic soil classification: the VfZ matrix*. Bull. Earthquake Eng., **12**, 735-754, doi: 10.1007/s10518-013-9543-3.

Denolle M.A., Fan W. and Shearer P.M.; 2015: *Dynamic of the 2015 M 7.8 Nepal earthquake*. Geophys. Res. Lett., **42**, 7467-7475.

Dhakal Y.P., Kubo H., Suzuki W., Kunugi T., Aoi S. and Fujiwara H.; 2016: *Analysis of strong ground motions and site effects at Kantipath, Kathmandu, from 2015 Mw 7.8 Gorkha, Nepal, earthquake and its aftershocks*. Earth, Planets Space, **68**, 58, doi: 10.1186/s40623-016-0432-2.

Dill H.G., Kharel B.D., Singh V.K., Piya B. and Geyh M.; 2001: *Sedimentology and paleogeographic evolution of the intermontane Kathmandu basin, Nepal, during the Pliocene and Quaternary. Implications for formation of deposits of economic interest*. J. Asian Earth Sci., **19**, 777-804.

Dixit A., Ringler A., Sumy D.F., Cochran E.S., Hough S.E., Martin S.S., Gibbons S., Luetgert J.H., Galetzka J., Shrestha S.N., Rajaure S. and McNamara D.E.; 2015: *Strong-Motion observations of the M 7.8 Gorkha, Nepal, earthquake sequence and development of the N-SHAKE strong-motion network*. Seismol. Res. Lett., **86**, 1533-1539, doi: 10.1785/0220150146.

Fäh D., Kind F. and Giardini D.; 2001: *A theoretical investigation of average H/V ratios*. Geophys. J. Int., **145,** 535-549.

Field E. and Jacob K.; 1993: *The theoretical response of sedimentary layers to ambient seismic noise*. Geophys. Res. Lett., **20**, 2925-2928.

Fujii R., Harutaka S. and Norio M.; 2004: *Fluctuation of Indian monsoon during the last glacial period revealed by pollen analysis of Kathmandu Basin sediments, Nepal Himalaya*. In: Extended Abstracts, 19th Himalaya-Karakorum-Tibet Workshop, Niseko, Japan, pp. 133-134.

Galetzka J., Melgar D., Genrich J.F., Geng J., Owen S., Lindsey E.O., Xu X., Bock Y., Avouac J.-P., Adhikari L.B., Upreti B.N., Pratt-Sitaula B., Bhattarai T.N., Sitaula B.P., Moore A., Hudnut K.W., Szeliga W., Normandeau J., Fend M., Flouzat M., Bollinger L., Shrestha P., Koirala B., Gautam U., Bhatterai M., Gupta R., Kandel T., Timsina C., Sapkota S.N., Rajaure S. and Maharjan N.; 2015: *Slip pulse and resonance of the Kathmandu basin during the 2015 Gorkha earthquake, Nepal*. Sci., **349**, 1091-1095, doi: 10.1126/science.aac6383.

Hossler T., Bollinger L., Sapkota S.N., Lave J., Gupta H.K. and Kandel T.P.; 2015: *Surface ruptures of large Himalayan earthquakes in western Nepal: evidence along a reactivated strand of the Main Boundary Thrust*. Earth Planet. Sci. Lett., **434**, 187-196.

Hough S.E. and Bilham R.; 2008: *Site response of the Ganges basin inferred from re-evaluated macroseismic observations from the 1897 Shillong, 1905 Kangra, and 1934 Nepal earthquakes*. J. Earth Syst. Sci., **117,** 773-782.

Igarashi Y., Yoshida M. and Tabata H.; 1988: *History of vegetation and climate in the Kathmandu valley*. Proc. Indian natn. Sci. Acad., **54**, 550-563.

Jouanne F.; 2015: *The 25 April Gorka earthquake Pre-, co- and post-deformations from GPS measurement*. In: Tiwari M., Kumar K., Philip G., Rao D.R. and Suresh N. (eds), 30th Himalaya-Karakoram-Tibet Workshop, WIHG, Dehradun, India, pp. 108-110, <www.wihg.res.in>.

Khadka M.S.; 1993: *The groundwater quality situation in alluvial aquifers of the Kathmandu Valley, Nepal*. AGSO J. Aust. Geol. Geophys., **14**, 207-211.

Konno K. and Omachi T.; 1998: *Ground-Motion characteristics estimated from spectral ratio between horizontal and vertical components of microtremors*. Bull. Seismol. Soc. Am., **88**, 228-241.

Kuwahara Y., Raj Paudel M., Maki T., Fujii R. and Sakai H.; 2004: *Variations of paleoclimate and paleoenvironment during the last 40 kyr recorded in clay minerals in the Kathmandu Basin sediments*. In: Extended Abstracts, 19th Himalaya-Karakorum-Tibet Workshop, Niseko, Japan, pp. 190-191.

Lachet C. and Bard P.-Y.; 1994: *Numerical and theoretical investigations on the possibilities and limitations of Nakamura's technique*. J. Phys. Earth, **42,** 377-397.

Lermo J., Rodriguez M. and Singh S.K.; 1988: *Natural periods of sites in the valley of Mexico from microtremors measurements and strong motion data*. Earthquake Spectra. **4**, 805-814.

Louie J.; 2001: *Faster, better: shear-wave velocity to 100 meters depth from refraction microtremor arrays*. Bull. Seismol. Soc. Am., **91**, 347-364.

Lunedei E. and Albarello D.; 2009: *On the seismic noise wave field in a weakly dissipative layered Earth*. Geophys. J. Int., **177**, 1001-1014, doi: 10.1111/j.1365-246X.2008.04062.x.

Mampuku M., Yamanaka T., Uchida M., Fujii R. and Maki T.; 2008: *Changes in $C_3/C_4$ vegetation in the continental interior of the central Himalayas associated with monsoonal paleoclimatic changes during the last 600 kyr*. Clim. Past, **4**, 1-9, doi: 10.5194/cp-4-1-2008.

MoHA; 2015: *Nepal Earthquake 2015: Disaster Recovery and Reconstruction InformationPlatform (NDRRIP)*. The Ministry of Home Affairs (MoHA) Government of Nepal, <drrportal.gov.np/ndrrip/main.html>.

Molnar S., Onwuemeka J. and Adhikari S.; 2017: *Use of ambient vibration methods for post-earthquake geotechnical reconnaissance in Kathmandu, Nepal*. In: Proc. 16th World Conference on Earthquake, Santiago, Chile, Paper n. 1869, 10 pp.

Moribayashi S. and Maruo Y.; 1980: *Basement topography of the Kathmandu Valley, Nepal - an application of the gravitational method to the survey of a tectonic basin in the Himalaya*. J. Jpn Soc. Eng. Geol., **21**, 30-37.

Mougnier J.L., Huyghe P., Gajurel A.P. and Becel D.; 2005: *Frontal and piggy-back seismic ruptures in the external thrust belt of western Nepal*. J. Asian Earth Sci., **25**, 707-717.

Mukunda R.P. and Sakai H.; 2008: *Stratigraphy and depositional environments of basin-fill sediments in southern Kathmandu Valley, central Nepal*. Bull. Dept. Geol., Tribhuvan University, Kathmandu, Nepal, **11**, 61-70.

Nakamura Y.; 1989: *A method for dynamic characteristic estimation of subsurface using microtremors on the ground surface*. Quart. Rep. Railway Tech. Res. Inst., **30,** 25-33.

Nogoshi M. and Igarashi T.; 1971: *On the amplitude characteristics of microtremor (Part 2)*. J. Seismol. Soc. Jpn., **24**, 26-40.

NSET; 2015: *Gorkha earthquake: intensity maps*. <www.nset.org.np/eq2015/intensity_maps.php>.

Otha Y., Kagami H., Goto N. and Kudo K.; 1978: *Observation of 1-to-5 second microtremors and their applications to earthquake engineering. Part I: Comparision with long-period accelerations at Tokachi-Oki earthquake of 1968*. Bull. Seismol. Soc. Am., **68**, 767-779.

Pandey M.R., Tandukar R.P., Avouac J.P., Lavé J. and Massot J.P.; 1995: *Interseismic strain accumulation on the Himalayan crustal ramp (Nepal)*. Geophys. Res. Lett., **22**, 751-754.

Parolai S., Bormann P. and Milkerei C.; 2001: *Assessment of the natural frequency of the sedimentary cover in the Cologne area (Germany) using noise measurements*. J. Earthquake Eng., **5**, 541-564.

Paudayal K.N.; 2011: *Palynological assemblages from the Late Pleistocene sediments of the Patan Formation in Kathmandu Valley and their climatic implications*. Bull. Dept. Geol., Tribhuvan University, Kathmandu, Nepal, **14**, 59-66.

Paudyal Y.R., Bhandary N.P. and Yatabe R.; 2012: *Seismic microzonation of densely populated area of Kathmandu Valley of Nepal using microtremors observations*. Earthquake Eng., **16**, 1208-1229.

Paudyal Y.R., Yatabe R., Bhandary N.P. and Dahal R.K.; 2013: *Basement topography of the Kathmandu Basin using microtremor observation*. J. Asian Earth Sci., **62**, 627-637, doi: 10.1016/j.jseaes.2012.11.011.

Pettenati F., Sirovich L. and Bjerrum L.; 2017: *Fault sources and kinematics of the 1897 Assam (MW8.1) and the 1934 Nepal (MS8.2) earthquakes retrieved by KF-NGA inversion and their seismotectonic implications*. Bull. Seismol. Soc. Am., **107**, 2480-2489, doi: 10.1785/01201160391.

Rupakhety R., Olafsson S. and Halldorsson B.; 2017: *The 2015 Mw 7.8 Gorkha Earthquake in Nepal and its aftershocks: analysis of strong ground motion*. Bull. Earthquake Eng., **15**, 2587-2616, doi: 10.1007/s10518-017-0084-z.

Sakai H., Fujii R., Kuwahara Y., Upreti B.N. and Shrestha S.D.; 2001: *Core drilling of the basin-fill sediments in the Kathmandu Valley for palaeoclimatic study: preliminary results, Nepal*. J. Nepal Geol. Soc., **25**, 9-18.

Sakai H., Gajurel A.P., Upreti B.N., Tabata H., Ooi N. and Kitagawa H.; 2008: *Revised lithostratigraphy of fluvio-lacustrine sediments comprising northern Kathmandu basin in central Nepal*. J. Nepal Geol. Soc., **37**, 25-44.

Sapkota N.S., Bollinger L., Klinger Y., Tapponnier P., Gaudemer Y. and Tiwar D.; 2013: *Primary surface ruptures of the great Hiamlayan earthquakes in 1934 and 1255*. Nature Geosci., **6**, 71-76, doi: 10.1038/NGEO1669.

SESAME, 2004: *Guidelines for the implementation of the H/V spectral ratio technique on ambient vibrations: measurements, processing and interpretation*. SESAME European research project WP12 - Deliverable D23.12, European Commission - Research General Directorate, Bruxelles, Belgio, <ftp.geo.uib.no/pub/seismo/SOFTWARE/SESAME/USER-GUIDELINES/SESAME-HV-User-Guidelines.pdf>.

Singh R.P., Aman A. and Prasad Y.J.J.; 1996: *Attenuation relations for strong seismic ground motion in the Himalayan Region*. Pure Appl. Geophys., **147**, 161-180.

Sirovich L., Pettenati F., Cavallini F. and Bobbio M.; 2002: *Natural-neighbor isosismals*. Bull. Seismol. Soc. Am., **92**, 1933-1940.

Stöklin J. and Bhattarai K.D.; 1977: *Geology of the Kathmandu Area and central Mahabharat Range, Nepal*. In: Himalaya Report, Department of Mines and Geology, Kathmandu, Nepal, 86 pp.

Szeliga W., Hough S., Martin S. and Bilham R.; 2010: *Intensity, magnitude, location, and attenuation in India for felt earthquakes since 1762*. Bull. Seismol. Soc. Am., **100**, 570-584, doi: 10.1785/0120080329.

Takai N., Shigefuji M., Rajaure S., Bijukchhen S., Ichiyanagi M., Dhital M.R. and Sasatani T.; 2016: *Strong ground motion in the Kathmandu Valley during the 2015 Gorkha, Nepal, Earthquake*. Earth Planets Space, **68**, 10, doi: 10.1186/s40623-016-0383-7.

Trevisani S., Boaga J., Agostini L. and Galgaro A.; 2017: *Insights into bedrock surface morphology using low-cost passive seismic surveys and integrated geostatistical analysis*. Sci. Total Environ., **578**, 186-202, doi: 10.1016/j.scitotenv.2016.11.041.

Wesnousky S.G., Kumahara Y., Chamlagain D., Pierce I.K., Karki A. and Gautam D.; 2017: *Geological observations on large earthquakes along the Himalayan frontal fault near Kathmandu*. Nepal Earth Planet. Sci. Lett., **457**, 366-375, doi: 10.1016/j.epsl.2016.10.006.

*Corresponding author:*     Franco Pettenati
                            Istituto Nazionale di Oceanografia e di Geofisica Sperimentale - OGS
                            Borgo Grotta Gigante 42c, 34010 Sgonico (TS), Italy
                            Phone: +39 040 2140317; e-mail: fpettenati@inogs.it